

SPECIAL PROJECT PROGRESS REPORT

Reporting year 2019

Project Title: Towards Cloud-Resolving Climate Simulations

Computer Project Account: spnlcrom

Principal Investigator(s): Daan Crommelin, Pier Siebesma, Gijs van den Oord, Fredrik Jansson, Maria Chertova

Affiliation: Centrum Wiskunde & Informatica (Crommelin, Jansson), KNMI and TU Delft (Siebesma), Netherlands eScience Center (van den Oord, Chertova)

Name of ECMWF scientist(s) collaborating to the project
(if applicable) Glenn Carver has helped us with running OpenIFS and by providing initial states for the simulations

Start date of the project: 1/1/2017

Expected end date: 31/12/2019

Computer resources allocated/used for the current year and the previous one
(if applicable)

Please answer for all project resources

		Previous year		Current year	
		Allocated	Used	Allocated	Used
High Performance Computing Facility	(units)	15M	11.2M	15M	8.3M
Data storage capacity	(Gbytes)	100000		100000	18T/\$SCRATCH, 9.3T/tape

Summary of project objectives (10 lines max)

The overarching goal of this project is to come to a better understanding of cloud-climate feedbacks, leading to reduced uncertainty in climate sensitivity estimates. To achieve this, we pursue a computational strategy of developing 3-dimensional superparameterization (3dSP) by embedding 3-d convection-resolving Large Eddy Simulation (LES) models in each grid column of a global model (OpenIFS). The LES models are embedded as a two-way nesting (or two-way coupling): the global model column state drives the LES model, and the LES feeds back to the global model. The nested LES models replace traditional convection parameterization schemes in the global model columns. We work with DALES, the Dutch Large Eddy Simulation model, as the convection-resolving LES. The computer resources of this special project are intended for performing simulations with the coupled (OpenIFS-DALES) 3dSP model for test cases including a cold air outbreak case (previously subject of the WGNE Grey Zone project).

Summary of problems encountered (10 lines max)

In 2017 we found out that AMUSE does not work well with the Cray MPI which is installed on the ECMWF Cray, the reason being that when AMUSE spawns worker processes it launches them using `MPI_Comm_spawn()`, which the Cray MPI does not support. We solved this problem with a work-around where all workers are launched at the start of the simulation in a regular MPI job, after which the appropriate MPI communicators are created. This works for us, since we know ahead of time how many workers are needed for a particular simulation. Supposedly new versions of the Cray MPI will include `MPI_Comm_spawn()`. We are still using the work-around with pre-launched worker codes.

Summary of plans for the continuation of the project (10 lines max)

- Analyze and improve the performance of the coupled model.
- The Python interface to the DALES (LES-based, local, cloud-resolving model) will be presented as a software paper, and is going to be used in teaching, for interactive control of the DALES model.
- Beyond the current project, the superparameterized OpenIFS-model will be used as a one example application in a project on multiscale modelling (VECMA).
- Investigate how the model coupling scheme can be improved, in particular to account for variability on scales smaller than the global model's grid size, which affects advection of clouds from one superparameterized grid point to another.

List of publications/reports from the project with complete references

F. Jansson, G. van den Oord, I. Pelupessy, J. H. Grönqvist, A. P. Siebesma, D. Crommelin (2019) *Regional superparameterization in a Global Circulation Model using Large Eddy Simulations*, submitted.

Conference papers:

Pelupessy I. et al. (2019) *Creating a Reusable Cross-Disciplinary Multi-scale and Multi-physics Framework: From AMUSE to OMUSE and Beyond*. In: Rodrigues J. et al. (eds) Computational Science – ICCS 2019. Lecture Notes in Computer Science, vol 11539. Springer. **DOI:** 10.1007/978-3-030-22747-0_29

Conference abstracts:

Fredrik Jansson, Gijs van den Oord, Inti Pelupessy, Maria Chertova, Pier Siebesma, and Daan Crommelin (2019) [On the regional superparametrization of OpenIFS by 3D LES models](#), Geophysical Research Abstracts, Vol. 21, EGU2019-11303

Jansson, F.R, van den Oord, G, Siebesma, A.P, & Crommelin, D.T. (2018). *Resolving clouds in a global atmosphere model - a multiscale approach with nested models*. In Proceedings - IEEE 14th International Conference on eScience, e-Science 2018. DOI:10.1109/eScience.2018.00043

Daan Crommelin , Pier Siebesma, Fredrik Jansson, Gijs van den Oord, Inti Pelupessy, Johanna Grönqvist, Maria Chertova (2019). *Regional Superparameterization with LES*. In Mathematisches Forschungsinstitut Oberwolfach Report No. 7/2019. DOI: 10.4171/OWR/2019/7

Fredrik Jansson, Gijs van den Oord, Inti Pelupessy, Maria Chertova, Johanna Grönqvist, Daan Crommelin, Pier Siebesma (2019). *High-resolution regional superparameterization of OpenIFS with DALES*. In UCP2019 - Understanding Clouds and Precipitation/ Book of Abstracts.

Summary of results

Progress July 2018 – June 2019

A comprehensive article describing the superparameterization setup and initial results has been submitted to JAMES and is currently under revision. The submitted preprint is attached to this report. We quote its abstract below:

“As an explorative step towards global Large Eddy Simulations, we investigate using comprehensive three dimensional Large Eddy Simulations as a superparameterization that can replace all traditional parameterizations of atmospheric processes that are currently used in global models. We present the technical design for a replacement of the parameterization for clouds, convection, and turbulence of the global atmospheric model of the European Centre for Medium-Range Weather Forecasts (ECMWF) by the Dutch Atmospheric Large Eddy Simulation (DALES) model. The model coupling consists of bidirectional data exchange between the global model and the high-resolution Large Eddy Simulation (LES) models embedded within the columns of the global model. Our setup allows for selective superparameterization, i.e. for applying superparameterization in local regions selected by the user, whilst keeping the standard parameterization of the global model intact outside this region. Our design allows the LES instances to run concurrently. First simulation results, employing this design, demonstrate the potential of our approach”. [from Jansson et al., 2019]

The code for the coupling of OpenIFS and DALES is made available on GitHub, details can be found in the article. Also, the separate Python interfaces to OpenIFS and to DALES have been included in the official OMUSE repository.

Furthermore, many bug fixes and improvements for DALES developed in this project have been included in the newly released DALES 4.2.

Regional superparameterization in a Global Circulation Model using Large Eddy Simulations

Fredrik Jansson¹, Gijs van den Oord², Inti Pelupessy², Johanna H. Grönqvist³, A. Pier Siebesma^{4,5}, Daan Crommelin^{1,6}

¹Centrum Wiskunde & Informatica, Amsterdam

²Netherlands eScience Center, Amsterdam

³Åbo Akademi University, Turku, Finland

⁴Royal Netherlands Meteorological Institute, de Bilt

⁵Delft University of Technology, Delft

⁶Korteweg-de Vries Institute, University of Amsterdam, Amsterdam

Key Points:

- Efficient Implementation of a Large Eddy Simulation (LES) based superparameterization into a global circulation model.
- Flexibility on the position and the size of the superparameterized area.
- Promising evaluation of the first results of an LES-based superparameterized simulation.

Corresponding author: Fredrik Jansson, jansson@cwi.nl

Abstract

As an explorative step towards global Large Eddy Simulations, we investigate using comprehensive three dimensional Large Eddy Simulations as a superparameterization that can replace all traditional parameterizations of atmospheric processes that are currently used in global models. We present the technical design for a replacement of the parameterization for clouds, convection, and turbulence of the global atmospheric model of the European Centre for Medium-Range Weather Forecasts (ECMWF) by the Dutch Atmospheric Large Eddy Simulation (DALES) model. The model coupling consists of bidirectional data exchange between the global model and the high-resolution Large Eddy Simulation (LES) models embedded within the columns of the global model. Our setup allows for selective superparameterization, i.e. for applying superparameterization in local regions selected by the user, whilst keeping the standard parameterization of the global model intact outside this region. Our design allows the LES instances to run concurrently. First simulation results, employing this design, demonstrate the potential of our approach.

1 Introduction

An accurate representation of clouds and convection in global weather and climate models and their interaction with the large-scale circulation remains one of the main challenges in atmospheric modeling. Uncertainties in the representation of clouds and convection are the prime sources of uncertainty in climate model sensitivity, and major contributors to longstanding biases in the representation of the precipitation patterns in current climate and their projections in future climate (Bony et al., 2015; Schneider, Teixeira, et al., 2017).

Cloud related processes occur over a wide range of scales ranging from cloud droplet formation at the micrometer scale to cloud convective updrafts and downdrafts that can be as large as 10 km, from which organized mesoscale systems can emerge extending over hundreds of kilometers. Current operational global models operate at numerical resolutions in the range of 10-100 km. As a consequence, cloud and convective processes are numerically not resolved and their impact on the resolved state is instead approximated by parameterizations, causing uncertainties of these unresolved processes.

The problem of parameterized clouds and convection is largely avoided when using Large Eddy Simulations (LES). The paradigm of LES is based on the idea that small unresolved turbulent eddies can be faithfully parameterized in terms of the resolved large eddies by making use of the self-similar structure of turbulence in the inertial subrange. The atmospheric inertial subrange is bounded by the depth of the atmospheric boundary layer which has a typical depth of 1 kilometer, indicating that a minimum resolution of $O(100\text{ m})$ is required to numerically resolve the relevant turbulence, convection, and cloud dynamics.

Two obvious but challenging pathways for improving the representation of clouds and convection in global models are either increasing the resolution of existing global models to turbulence-resolving scales, or extending the spatial domains of Large Eddy Simulations until a global scale is reached. Regarding the latter approach, realistic multi-day large eddy simulations have been reported on domains approaching 1000 km^2 (Schalkwijk et al., 2015; Heinze et al., 2017). Global multiday simulations are approaching the 1 kilometer resolution scale and are capable of partly resolving the cloud dynamics and therefore usually referred to as global cloud resolving models (CRMs) (Miyamoto et al., 2013; Bretherton & Khairoutdinov, 2015). Global CRMs form an interesting playground to explore the interaction between the global circulation and the resolved moist convective systems, but one should also bear in mind that for resolutions used in global CRMs (1-5km), atmospheric turbulence and boundary layer clouds remain essentially unresolved.

66 A different pathway is offered by superparameterization (SP) (Grabowski & Smo-
 67 larkiewicz, 1999; Grabowski, 2001, 2004; Khairoutdinov & Randall, 2001; Khairoutdi-
 68 nov et al., 2005), where existing global and local cloud resolving models are coupled. The
 69 common set-up for SP is to replace deep convection and cloud parameterization schemes
 70 in every model column of the global model by a CRM. Because of computational con-
 71 straints, the CRMs used in SP are mostly two-dimensional (2D). A 3D CRM was used
 72 by Khairoutdinov et al. (2005), but the grid of the CRM was still very coarse and lim-
 73 ited to 8×8 columns. Jung and Arakawa (2010) present a quasi-3D SP where the global
 74 models grid points are connected by narrow corridors consisting of 3D local models. An
 75 overview of other simulation studies with SP is provided by Tao and Chern (2017). Like
 76 global CRMs however, these SP approaches traditionally use horizontal resolution of 1-
 77 4 km and coarse vertical resolutions, and still require additional parameterizations for
 78 boundary layer clouds and turbulence.

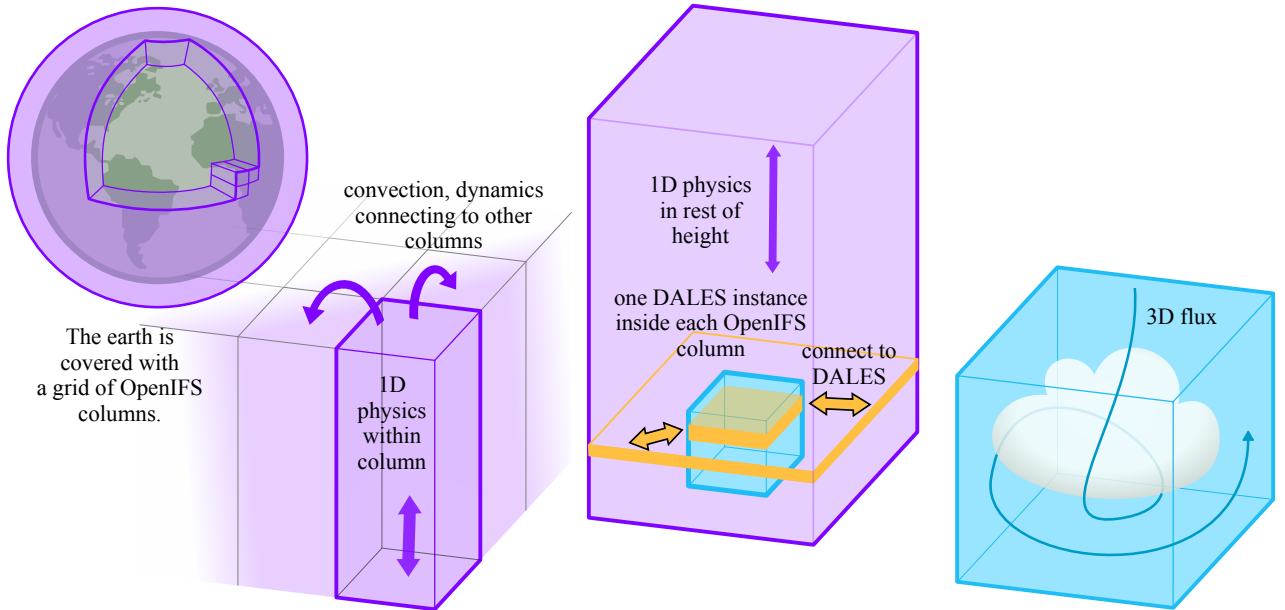
79 Recently, a variation on superparameterization has been proposed (Grabowski, 2016),
 80 where the resolution of local CRMs becomes fine enough to be turbulence resolving. Parishani,
 81 Pritchard, Bretherton, Wyant, and Khairoutdinov (2017) included LES models with a
 82 fine spatial horizontal resolution (250m) and 125 vertical levels in their global model. How-
 83 ever, to be able to run the global model with SP, the LESs used small domains (8×8
 84 columns, i.e. $2 \text{ km} \times 2 \text{ km}$) covering only a small fraction of the domain of a single col-
 85 umn of the global model.

86 Ideally, SP is carried out with a 3D high-resolution CRM that covers the full do-
 87 main of each global model column. To reduce the enormous computational cost of this
 88 (hypothetical) SP set-up, in the studies mentioned above either the 3D CRM is simpli-
 89 fied to 2D or quasi-3D, or the grid of each CRM is kept small (e.g. 8×8 horizontal).
 90 In the latter case, one can choose between high resolution on a small CRM domain (Parishani
 91 et al., 2017), or coarser resolution on a larger CRM domain (Khairoutdinov et al., 2005).

92 The SP approach that we will present in this study is different. Our aim is to use
 93 turbulence resolving resolutions on sufficiently large 3D-domains as a SP, in accordance
 94 with the resolution of the large-scale model. Computationally, this approach obviously
 95 does not allow SP to be applied globally. Therefore, rather than reducing the cost of the
 96 3D CRM as sketched above, our set-up creates the possibility to use SP only in a selected
 97 region, while leaving the regular (non-SP) parameterization in use outside this region.
 98 The motivation for this approach is simply that using 3D LES as a SP provides the best
 99 benchmark for conventional parameterizations.

100 The benefits of such a 3D LES-based SP in a conventional hydrostatic global model
 101 over a global LES or CRM have been discussed in Grabowski (2016). Computationally,
 102 it is attractive since all the local models can run independent from each other and only
 103 have to exchange mean profiles with the large-scale model. This allows an efficient im-
 104 plementation on massively parallel computer systems since all the SP models can run
 105 independently on separate cores. Further acceleration can be achieved by running the
 106 SP models sparser in space and time (Xing et al., 2009) or by varying the vertical res-
 107 olution of the SP models depending on cloud types that they need to resolve (Marchand
 108 & Ackerman, 2011). Conceptually there is also the advantage that the large-scale model
 109 can be formulated efficiently in a hydrostatic manner while the smaller scale LES based
 110 SP models can be conveniently expressed in an anelastic formulation. This way there
 111 is no need to find an appropriate soundproof compressible formulation of the dynamics
 112 on a global scale.

113 The drawback of any SP formulation is that it introduces a scale break at the res-
 114 olution scale of the large-scale model. This hinders the spectral transfer of variability
 115 across this scale and will potentially influence mesoscale organization. However, it also
 116 offers an excellent opportunity to explore the effect of such a scale break which is present
 117 in every operational large-scale model.



128 **Figure 1.** Overview of the superparameterized model. Some grid columns of the global model
 129 OpenIFS (purple), are selected for superparameterization. Each of them is coupled to a local
 130 DALES model (blue), which resolves clouds and convection in three dimension. The tendencies
 131 generated by these processes are fed back to the global model.

118 In this paper we will discuss the implementation and performance of the Dutch At-
 119 mospheric Large Eddy Simulation (DALES) model as a regional 3D LES based super-
 120 parameterization into the Open Integrated Forecast System (OpenIFS) developed at the
 121 European Centre for Medium-Range Weather Forecasts (ECMWF) (Carver & Vana, 2017).
 122 Section 2 describes the complete methodology of the coupling while Section 3 concen-
 123 trates more on the technical implementation. Section 4 presents results of a superparam-
 124 eterized atmospheric simulations over the Netherlands, comparisons with observations
 125 and an evaluation of the numerical performance. Section 5 contains conclusions, discus-
 126 sion, and outlook.

127 2 Methods

132 For coupling the global and cloud-resolving models, we follow the approach pre-
 133 sented by Grabowski (2004) and also (Khairoutdinov & Randall, 2001; Khairoutdinov
 134 et al., 2005). In the grid columns of the global model which are selected for superparam-
 135 eterization, a local, Large Eddy Simulation (LES) model is embedded as shown in Fig.
 136 1. The general idea is that for each coupled quantity, a forcing is introduced, which keeps
 137 the states of the two models consistent with each other. The coupling is bi-directional,
 138 so that the effects of clouds, turbulence and convection which are resolved in the local
 139 model are fed back to the global model.

140 Below, we summarize the coupling procedure, first in a simplified case where the
 141 two models are assumed to have similar vertical grid levels and to be formulated in terms
 142 of the same quantities. We then discuss the adaptations needed to couple models with
 143 different vertical levels and different physical quantities, as is the case for our set-up with
 144 coupling between DALES and OpenIFS.

145

2.1 Physical coupling of the models

146

147

148

149

150

151

152

153

We consider a 3D small-scale model embedded in a single column of the large-scale model. In earlier versions of the superparameterization scheme (Grabowski & Smolarkiewicz, 1999; Grabowski, 2001), the states of the large-scale and the small-scale models are relaxed towards each other, with a freely chosen time constant, which was taken as one hour. In the later scheme (Grabowski, 2004), the relaxation time constant is chosen equal to the time step of the large-scale model, making the models more tightly coupled. The aim is that for any coupled quantity Q , the horizontal slab average in the small-scale model at height z matches the value at the same height in the large-scale model:

$$Q(Z = z, t) = \langle q(x, y, z, t) \rangle. \quad (1)$$

154

155

156

157

158

Capital letters denote quantities in the large-scale model, lower-case letters denote the small-scale model. Q and q here may represent any of the prognostic variables, and the brackets $\langle \cdot \rangle$ denote a horizontal slab average over the domain of the local model. In the appendix we analyze to what extent the desired equality (1) can be achieved with the scheme from (Grabowski, 2004).

159

160

161

162

The coupled variables generally include the horizontal wind velocities, the temperature, and the specific humidity. As in earlier superparameterization works, the vertical velocities are left uncoupled. Since each local model is a closed system due to periodic boundary conditions, the horizontal average of the vertical velocity is zero.

163

164

165

166

The models are coupled by introducing additional forcings in both models, i.e. additional contributions to the time derivatives of the coupled quantities. F_Q represents a forcing that stems from q and acts on Q in the large-scale model, while f_q represents a forcing stemming from Q and acting on q in the small-scale model.

167

168

169

170

171

The time-stepping procedure is as follows. The large-scale model performs a single time step from time T to $T + \Delta T$, then the small-scale model is evolved over the same time interval, in multiple steps of length Δt . Before the time evolution of each model, forcings are calculated based on the difference between the most recently obtained states of the two models.

172

173

- (i) Given the state of both models at time T , represented by $Q(T)$ and $q(T)$, calculate forcings on the large-scale model

$$F_Q(T) = \frac{\langle q(T) \rangle - Q(T)}{\Delta T}. \quad (2)$$

174

- (ii) Time-step the large-scale model

$$Q(T + \Delta T) = Q(T) + \Delta T [A_Q(T) + S_Q(T) + F_Q(T)], \quad (3)$$

175

176

177

where $A_Q(T)$ represents advection terms and $S_Q(T)$ represents source terms during the step from T to $T + \Delta T$.

- (iii) Calculate the forcing on the small-scale model

$$f_q(T) = \frac{Q(T + \Delta T) - \langle q(T) \rangle}{\Delta T}. \quad (4)$$

178

- (iv) Time-step the small-scale model

$$q(T + \Delta T) = q(T) + \sum_{t=T}^{T+\Delta T} \Delta t [a_q(t) + s_q(t) + f_q(T)]. \quad (5)$$

179

180

181

The sums over t here schematically represent evolving the small-scale model over several time steps, with $a_q(t)$ denoting advection terms and $s_q(t)$ denoting source terms in the small-scale model.

182 This choice of forcings is such that they couple the advection and source terms between
 183 the models, see also Grabowski (2004). In particular, one can show that

$$F_Q(T + \Delta T) = \frac{1}{\Delta T} \sum_{t=T}^{T+\Delta T} \Delta t \langle a_q(t) + s_q(t) \rangle, \quad (6)$$

184 and

$$f_q(T) = A_Q(T) + S_Q(T), \quad (7)$$

185 so that the forcings on the small-scale model equals the advective and source tendencies
 186 in the large-scale model and vice versa. Thus, each physical process should be taken into
 187 account in one of the models, but not in both. Otherwise the contribution will be counted
 188 twice. As is shown in the appendix, the equality (1) is satisfied exactly if all physical pro-
 189 cesses are accounted for in one model and none in the other: if $\langle a_q(t) + s_q(t) \rangle = 0$ for
 190 all t then $Q(T) = \langle q(T) \rangle$, whereas if $A_Q(T) + S_Q(T) = 0$ then $Q(T + \Delta T) = \langle q(t) \rangle$.

191 The Grabowski scheme does not explicitly describe the superparameterization pro-
 192 cedure for the sequential-splitting method in the global model, which are used in the col-
 193 umn physics routines in OpenIFS. In this algorithm the physics processes are ordered
 194 by decreasing time scales and every tendency is calculated with updated fields as its in-
 195 put, so that the tendencies of slower processes contribute to the evaluation of tenden-
 196 cies due to faster processes. We preserve this procedure by inserting the coupling to the
 197 local models at the stage in the OpenIFS time step where the parameterizations we sub-
 198 stitute are evaluated, namely turbulence, convection and cloud schemes as shown in Fig.
 199 2.

200 2.2 Interpolation and change of variables

201 The coupling scheme outlined so far is the standard superparameterization scheme
 202 as described in the references - where the vertical grids are assumed to be the same in
 203 the two models, and the models are formulated in the same variables. In our case of cou-
 204 pling OpenIFS and DALES, neither of these assumptions can be made, requiring a few
 205 extra steps in the model coupling. The two models may use different vertical grids, typ-
 206 ically the local model has a denser grid than the global model, and will not extend be-
 207 yond the tropopause. OpenIFS is formulated in so-called hybrid sigma pressure coordi-
 208 nates; in our test cases we used 90 vertical levels extending up to roughly 80 km. For
 209 DALES we typically used a vertical spacing of 25 m, extending up to 4 km. To exchange
 210 vertical profiles of quantities between global and the local models we use linear interpo-
 211 lation along the z-axis. We convert the OpenIFS hybrid model level profiles to altitude
 212 by fetching the full- and half-level pressure profiles P_f , P_h and using the hydrostatic ap-
 213 proximation to determine the height of each layer:

$$dZ = \frac{-R_d T [1 + (R_v/R_d - 1)Q_V - (Q_L + Q_I)]}{g_0 P_f} dP. \quad (8)$$

214 Here, $R_d \approx 287.04$ J/kg K is the gas constant for dry air, $R_v \approx 461.5$ J/kg K is the
 215 gas constant for water vapor, and g_0 is the acceleration due to gravity. Q_V is the wa-
 216 ter vapor specific humidity, while Q_L and Q_I are the specific humidities of liquid water
 217 and ice. Above the vertical extent of the DALES models we set the forcings F_Q on the
 218 global model to zero.

221 Furthermore, the two models are formulated using different prognostic variables.
 222 The coupling thus requires a variable conversion step. Table 1 lists the quantities that
 223 are coupled between the two models, the conversions required are described in detail be-
 224 low.

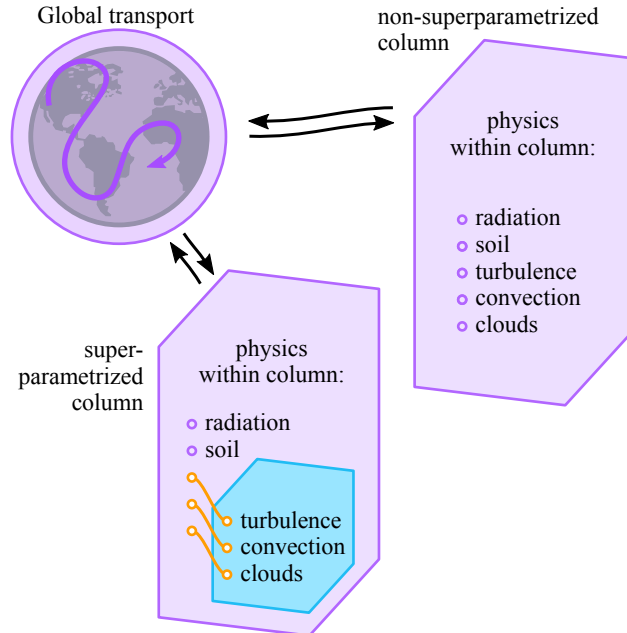
OpenIFS quantities

symbol	internal array name	description	unit	coupling direction
U, V	GMV	horizontal velocity	m/s	bidirectional
T	GMV	temperature	K	bidirectional
Q_V	GFL	water vapor specific humidity	kg/kg	bidirectional*
Q_L	GFL	liquid water specific humidity	kg/kg	bidirectional*
Q_I	GFL	ice water specific humidity	kg/kg	bidirectional*
Z_{0M}, Z_{0H}	ZAZOM, ZAZOH	surface roughness	m	output
\mathcal{F}_{SH}	PDIFTQ	specific humidity flux	kg/m ² s	output
\mathcal{F}_{QL}	PDIFTL	liquid water specific humidity flux	kg/m ² s	output
\mathcal{F}_{QI}	PDIFTI	ice specific humidity flux	kg/m ² s	output
\mathcal{F}_{TS}	PDIFTS	sensible heat flux	W/m ²	output
P_S	GMVS	surface pressure	Pa	output
A	GFL	cloud fraction	-	input

DALES quantities

symbol	variable name	description	unit	coupling direction
u, v	u0, v0	horizontal velocity	m/s	bidirectional
θ_l	thl0	liquid water potential temperature	K	bidirectional
q_t	qt0	specific humidity	kg/kg	input
q_v		water vapor specific humidity	kg/kg	output
q_L		liquid water specific humidity	kg/kg	output
q_I		ice water specific humidity	kg/kg	output
\mathcal{F}_q	wqsurf	specific humidity flux	kg/kg m/s	input
\mathcal{F}_{θ_l}	wtsurf	surface heat flux	K m/s	input
p_S		surface pressure	Pa	input
A		cloud fraction	-	output

219 **Table 1.** Quantities in OpenIFS and DALES used in the superparameterization scheme. *See
 220 text for the details of the humidity coupling.



225 **Figure 2.** In OpenIFS the column physics schemes for turbulence, convection and clouds are
 226 turned off in the superparameterized columns. These processes are instead handled by DALES.

227 For temperature, OpenIFS uses a regular temperature T , while DALES uses the
 228 liquid water potential temperature θ_l (Heus et al., 2010). For the conversion, we use

$$\theta_l \approx \frac{T}{\Pi} - \frac{L}{c_{pd}\Pi} q_c, \quad (9)$$

229 where q_c is the cloud condensate defined as the sum of cloud liquid water q_L and cloud
 230 ice q_I . The Exner function Π is defined as

$$\Pi(p) = \left(\frac{p}{p_0} \right)^{R_d/c_{pd}}. \quad (10)$$

231 Here $c_{pd} \approx 1004$ J/kg K is the specific heat of dry air at constant pressure.

232 For the humidity, DALES uses only a total humidity q_t as a prognostic variable.
 233 At every time step, q_t is partitioned into vapor, liquid and ice according to the local tem-
 234 perature. OpenIFS on the other hand, has separate prognostic variables for these quan-
 235 tities, Q_V for water vapor, Q_L for liquid water and Q_I for ice. When forcing DALES,
 236 the total humidity q_t is nudged towards the total humidity of the global model, calcu-
 237 lated as $Q_T = Q_V + Q_L + Q_I$. When coupling the humidities back to the global model,
 238 the diagnosed values of the DALES are used, so that each one of Q_V , Q_L , and Q_I is forced
 239 towards the horizontal average of the corresponding diagnosed quantity in DALES.

240 2.3 Surface scheme

241 Both DALES and OpenIFS contain a surface model which accounts for surface drag
 242 and for fluxes of heat and moisture between the atmosphere and the land or sea surface.
 243 We have chosen to use fluxes and surface roughness lengths calculated in OpenIFS, while
 244 letting Dales handle the effects these have on the atmosphere at the superparameterized
 245 grid points. In this way, we can rely on the land/sea mask, soil and vegetation data, and
 246 ocean wave model of OpenIFS, making it easy to set up a superparameterization any-
 247 where without having to supply detailed surface information.

248 We achieve this by having DALES run with prescribed roughness lengths and sur-
 249 face fluxes of moisture and heat. These quantities are retrieved from the OpenIFS at ev-
 250 ery time step. To avoid double counting of the surface fluxes, we disable the contribu-
 251 tion of the surface layer scheme in OpenIFS at the superparameterized grid points.

252 Since OpenIFS and DALES are built using quantities with different units (see ta-
 253 ble 1) unit conversions are necessary to consistently couple the surface fluxes. For the
 254 humidity flux, a scaling with the air density ρ is required:

$$\mathcal{F}_q = - \frac{\mathcal{F}_{QL} + \mathcal{F}_{QI} + \mathcal{F}_{SH}}{\rho}. \quad (11)$$

255 In the case of the heat flux, a conversion from heating power \mathcal{F}_{TS} in OpenIFS to liquid
 256 water potential temperature flux \mathcal{F}_{θ_l} in DALES is needed,

$$\mathcal{F}_{\theta_l} = - \frac{\mathcal{F}_{TS}}{\Pi(P_S)c_{pd}\rho}, \quad (12)$$

257 where Π is the Exner function given in Eq. (10). The models also differ in sign conven-
 258 tions: in DALES positive fluxes are upwards, into the atmosphere, while in OpenIFS pos-
 259 itive fluxes are downwards.

260 The coupling of the surface roughness lengths for momentum and heat provides a
 261 simple way to account for orographic variations and vegetation for the local models lo-
 262 cated over land, and for wave height for models above the sea.

263

2.4 Radiation, cloud condensate and cloud fraction

264

265

266

267

268

269

In our set-up, radiative heating and cooling in the atmosphere is currently handled only in the global model. This choice was mainly motivated from computational considerations as the handling of the radiation by DALES would result in a significant increase in computing time. DALES has the option to locally run the same radiation scheme as OpenIFS, so the option of diverting the radiation scheme to DALES is in principle available.

270

271

272

The cloud fraction A in the global model is derived by calculating the fraction of all the columns in DALES that contain a non-zero cloud condensate in the range from k_1 to k_2 . In formula, the cloud fraction A in the global model is given by

$$A = \frac{1}{i_{\max} j_{\max}} \sum_{i=1}^{i_{\max}} \sum_{j=1}^{j_{\max}} I^{k_2, k_1}(i, j) \quad (13)$$

273

274

275

276

277

278

279

280

where i and j are the horizontal grid-indices of DALES, and I is a indicator function which takes the value 1 in the case of any cloud condensate in the subcolumn between levels k_1 and k_2 at the horizontal coordinates i and j , and zero otherwise (Neggers et al., 2011). This choice for deriving A as a cloud fraction "defined-by-area", or projected cloud fraction is deliberate, because in OpenIFS it is implicitly assumed that clouds do not exhibit any subgrid variability within the vertical extent of the layer. Physically this implies that in the case where not all vertical levels in a DALES subcolumn are occupied with cloud condensate, it is averaged out over this subcolumn.

281

2.5 Other modeling choices

282

283

284

285

286

287

288

In DALES, the highest 25% of the model levels constitutes a so-called sponge layer. It removes fluctuations of wind, temperature and humidity, in order to damp gravity waves before they can reflect at the model top. The damping increases smoothly from the start of the sponge layer to the top of the system. There are several options for the damping mechanism. To be compatible with the superparameterization, we use a scheme where each quantity is relaxed towards the horizontal average of that quantity. Since this scheme preserves the horizontal average, it does not have a strong effect on the global model.

289

290

291

292

293

294

295

296

297

As in earlier superparameterization schemes, we do not couple the vertical velocity w between the two models. Due to the periodic boundary conditions of the local model, the horizontal average of $\langle w \rangle$ vanishes, which excludes the possibility of an explicit coupling. The effect of the large-scale vertical velocity on the prognostic fields in the global model is of course taken into account by the vertical advection and its effect is felt by the local model through the forcing as expressed by Eq. (4). Vice versa, the local model influences to thermodynamic state of the large-scale model and thereby indirectly also the large-scale vertical velocity within the hydrostatic formulation in a similar fashion that conventional convection parameterizations would do.

298

2.6 DALES horizontal extent and resolution

299

300

301

302

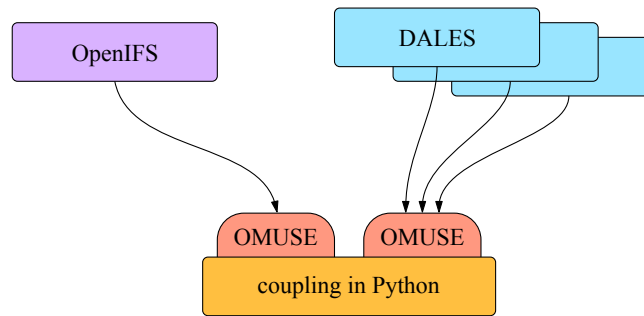
303

304

305

306

Since superparameterization does not involve lateral boundary forcings and all exchanged profiles involve bulk properties, the horizontal extent of the local models can in principle be chosen independently from the OpenIFS grid spacing. The DALES model size should be chosen to capture mesoscale structures as much as possible. However, the occurrence of such organization very much depends on the interaction with the large-scale dynamics and is often difficult to predict. For the horizontal DALES grid spacing we use an upper bound around 200 m; beyond this scale the DALES subgrid model can no longer accurately account for the unresolved turbulent motions.



317 **Figure 3.** Organization of the superparameterized simulation code, with a top-level coupling
 318 program communicating with the global model and a number of local model instances through
 319 OMUSE interfaces.

307 3 Implementation

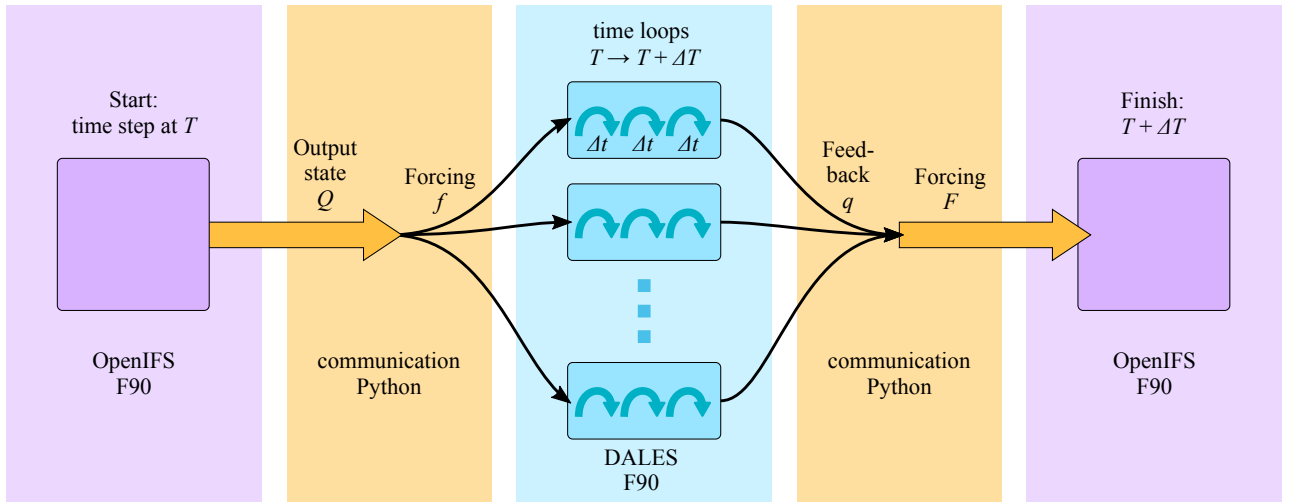
308 For superparameterization the OpenIFS model needs a bidirectional coupling to
 309 multiple instances of DALES, each one mapping to a different grid point of the global
 310 model. The central hypothesis in the design of the superparameterized simulation is that
 311 the bulk of the computing time in the coupled system is going to be spent during the
 312 time stepping of the local models. This is primarily because OpenIFS has a coarse grid
 313 and its numerical scheme allows large time steps, whereas the three-dimensional small-
 314 scale models are frequently restricted in their time step and thus have to perform many
 315 iterations to catch up with the global model. Hence it is important to allow the inde-
 316 pendent DALES instances to run concurrently on separate resources whenever available.

320 Previous superparameterization setups have generally embedded the local model
 321 in the column physics routines of the global model. This approach is feasible when su-
 322 perparameterization is applied uniformly in all model columns. In this project, we want
 323 to superparameterize only selected grid columns. Due to the organization of the OpenIFS
 324 program, it turns out to be difficult to embed DALES in the physics routine of selected
 325 columns, while letting the DALES instances run in parallel. For this reason, and also
 326 to keep the setup more modular, we settled on a different organization where the two
 327 model codes are kept as separate libraries, and an independent coupling program com-
 328 municates with them. The coupling program is written in Python, and communicates
 329 with the models, which are written mainly in Fortran, through a framework named OMUSE.
 330 (Pelupessy et al. (2017), see also S. Portegies Zwart et al. (2009); Pelupessy, F. I. et al.
 331 (2013); S. F. Portegies Zwart, McMillan, van Elteren, Pelupessy, and de Vries (2013)).
 332 This setup is illustrated in Fig. 3. In the following sections we explain the modifications
 333 made in OpenIFS and DALES, the role of the OMUSE framework and the coupling pro-
 334 gram.

335 3.1 Interface to OpenIFS

336 For the superparameterization coupler to be able to communicate with OpenIFS,
 337 a function interface is defined, with functions for initializing the model, setting tenden-
 338 cies, performing a time step and retrieving the model state.

339 In the original OpenIFS physics routines, the different physical processes are eval-
 340 uated in sequence, in order of decreasing characteristic time scale. The model uses a so-
 341 called sequential-splitting time stepping scheme, where the model state is updated af-
 342 ter each process, so that later processes operate on a state modified by the earlier ones.
 343 To preserve this process ordering in the superparameterized model, the coupling to the



366

Figure 4. Single time step of the superparameterized OpenIFS.

344

345

346

small-scale model should take place at the stage of replaced processes, namely where the (boundary layer) turbulence, the convection and the cloud scheme in the OpenIFS physics routine are called, as shown in figure 2.

347

348

349

350

351

352

353

354

The vertical physics processes in the original OpenIFS are evaluated for one column at a time in a single loop (actually the physical processes act on blocks of columns for optimal cache usage and vectorization, so the external loop runs over these sub-blocks). This means that the states of the superparameterized columns just before the cloud scheme is called, are not all available at the same time. Since these states are required for setting tendencies on the local models before their time evolution start, the local models cannot be time stepped in parallel with this organization of the OpenIFS physics routines.

355

356

357

358

359

360

361

362

363

364

365

To overcome this problem, and insert the model coupling at the right stage while keeping the local models parallel, we have split the OpenIFS time step into three global pieces: (i) a routine taking all prognostic fields to a state that has evolved dynamically and that incorporates all vertical physics effects up to the turbulence scheme, (ii) a routine that executes the original turbulence, convection and the cloud scheme on the grid columns not selected for superparameterization, and (iii) a routine that executes all remaining physical processes after the cloud scheme that is being executed subsequently, e.g. mass-fixers and diagnostics. We have also moved all stack-allocated arrays in the original loop over columns to heap-allocated data structures so that the global model keeps its state during the local model time-stepping. The original time step is therefore equivalent to the consecutive execution of these three routines.

367

368

369

370

371

372

373

374

To disable the OpenIFS cloud and convection schemes as well as the boundary layer turbulence scheme for the superparameterized grid points, we have introduced a global *superparameterization mask*. All parameterization routines are being executed, but for grid points where the mask is set, the tendencies from these processes are set to zero so that their effects are discarded. In this approach additional diagnostics arising from these parameterizations can still be used, e.g. the surface heat and momentum fluxes are still computed by the OpenIFS surface scheme and transferred to the local models to provide boundary conditions at the beginning of each superparameterization time loop.

375 **3.2 Interface to DALES**

376 A similar library interface was created for DALES, with functions for initializing
377 the model, setting tendencies, evolving the model until a given time, and fetching ver-
378 tical profiles of the model variables. Creating a library interface for DALES required less
379 involved changes than OpenIFS. The necessary changes were mainly to add interface func-
380 tions for tendencies and for retrieving horizontal averages of the variables.

381 **3.3 OMUSE coupling framework**

382 OMUSE (Pelupessy et al., 2017) is a framework for creating Python interfaces for
383 scientific codes written in various languages such as C or Fortran. With OMUSE, we cre-
384 ated Python versions of the function interfaces to OpenIFS and DALES described above.
385 OMUSE is MPI-aware, making it possible to transparently communicate with MPI-parallelized
386 models.

387 Through the OMUSE interface, both models can be controlled from a Python pro-
388 gram by calling Python functions. Internally, OMUSE translates these function calls to
389 Fortran function calls in the model codes, using MPI. Having MPI as the communica-
390 tion channel between the coupler and the models enable the models to be distributed
391 over multiple nodes in a cluster. Furthermore, OMUSE hides the parallel nature of the
392 models — every function in the OMUSE interface is collective over the MPI tasks of a
393 given model, freeing the coupler from dealing with lower-level details of how the mod-
394 els are parallelized. Using OMUSE is a way to keep the model modular, making it re-
395 latively easy to for example substitute DALES with another large eddy simulation code,
396 or even a single-column cloud model.

397 **3.4 The coupling code**

398 The superparameterization couplings described in section 2 have been implemented
399 in a Python program using the OMUSE interfaces to OpenIFS and DALES. Figure 4
400 shows the interaction of the different components during a time step of the combined model.

401 Our setup does not require communication between the DALES instances and OpenIFS
402 directly. All interactions are transferred through the coupling program, which fetches
403 and compares the model states and provides feedback to the models in the form of ten-
404 dencies. For localized superparameterization the communication overhead remains lim-
405 ited. Given the way the superparameterization coupling is formulated, no 3D fields need
406 to be exchanged — vertical profiles are sufficient. The cost of exchanging vertical pro-
407 files is generally small compared to the DALES runtime. Having a separate coupling code
408 in Python allows rapid prototyping and easy output of tailored diagnostics of the exchanged
409 tendencies. It also keeps the code modular and easier to maintain.

410 The OMUSE framework supports (at least on many HPC clusters) dynamic instan-
411 tiation of models; the coupling script is built to launch DALES instances within a user-
412 defined area at initialization, making it easy to select an area for superparameterization.
413 Furthermore, unit conversions and vertical interpolation of profiles are implemented in
414 the Python driver code. The system supports collection of basic performance statistics
415 and adding a spin-up period at the start of the simulation, where the DALES instances
416 are run for a specified time while being relaxed towards the vertical profiles of the OpenIFS
417 model.

418 We note that the precipitation is not yet coupled back from the local models to the
419 global model. The global model schemes which rely on the precipitation model for in-
420 put, the radiation and soil schemes, use the values computed with the global model’s pa-
421 rameterization. This may be of relevance for long runs, over time periods so long that
422 the soil properties are influenced by precipitation.

Coupling parameters

Number of DALES instances	42
Spin-up time	4 h
Duration	21 h

DALES parameters

Vertical resolution	25 m
Horizontal resolution	200 m
Vertical extent	4 km
Horizontal extent	40 km
Grid size	200 × 200 × 160
Time step	adaptive, ≈ 1...20 s

OpenIFS parameters

Grid	T511L91
Grid point distance	≈ 40 km
Initial state and	ERA-Interim
Sea Surface Temperature forcing	
Start time	2012-04-13 at 00:00 UTC
Time step	900 s

441

Table 2. Parameters used in the simulations

423

4 Results

424

425

426

427

428

429

Simulations using OpenIFS with a superparameterized setup over the Netherlands are performed for April 13 2012. This day was characterized by a west-northwesterly flow steered by a low over the Northern part of the North Sea. Clear skies are observed over the relatively cold water of the North Sea but convection developed when the cold air was advected from the North Sea over the Netherlands resulting in developing shallow cumulus clouds between 1 and 3 km over land.

430

431

432

433

434

435

436

437

438

439

440

The OpenIFS initial state was constructed by interpolation from the reanalysis dataset ERA-Interim (Dee et al., 2011). The local models were initialized with the vertical profiles of their corresponding grid points in the global model, with noise added in the horizontal direction to break the symmetry. After initialization, a spin-up of the local models was performed, where they were run for 4 hours while being relaxed towards the state of the global model. After spin-up the actual simulation was started, and the global and local models were time-stepped together as described in section 2. OpenIFS was run with a T511L91 grid in all cases, giving a distance between neighboring grid points of about 40 km. The simulation parameters are summarized in table 2. For the superparameterized run, we choose the extent of the DALES domains to match the grid point distance in OpenIFS.

442

4.1 Cloud cover

448

449

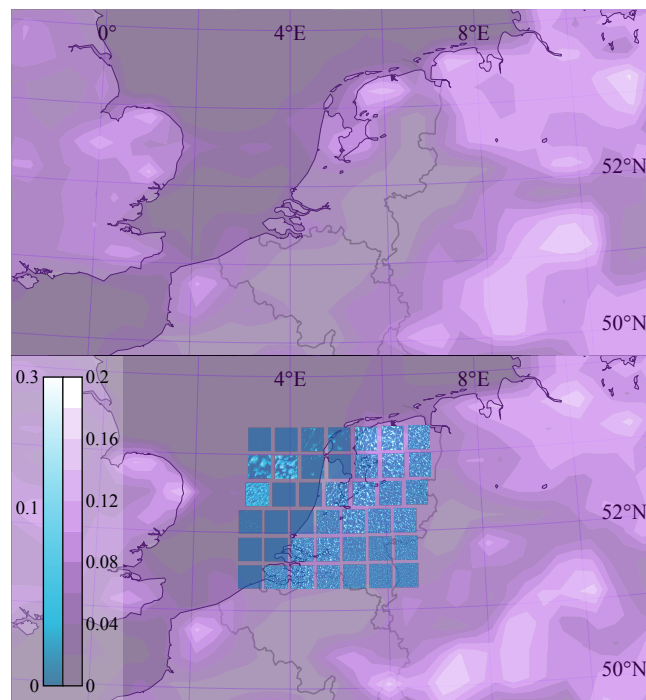
450

451

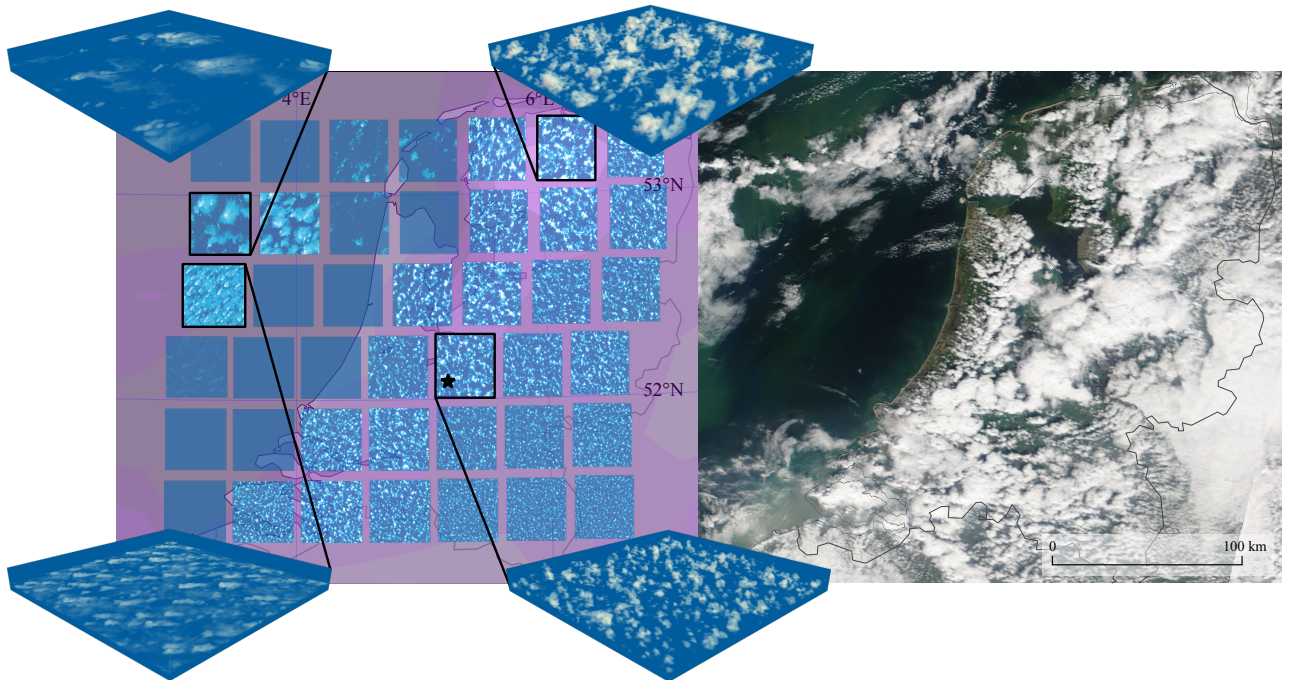
452

453

We compare the appearance of the cloud fields from the simulation with satellite images and with results from the unmodified OpenIFS. We also show vertical profiles of temperature, humidity, and cloud liquid water from the superparameterized run, and compare them with profiles from the unmodified OpenIFS, from the ERA-5 reanalysis and from a radiosonde observation. A full validation of the superparameterized model remains beyond the scope of this work.



443 **Figure 5.** A superparameterized simulation over the Netherlands (bottom), compared to the
444 same simulation run in standard OpenIFS (top). DALES instances are shown in blue, over a
445 background showing the OpenIFS state in purple. Cloudiness (liquid water path) is shown in
446 shades of white for both models. The state shown is for the time 2012-04-13 11:35 UTC; the
447 simulation was started at midnight the same date, with a state from ERA-Interim.



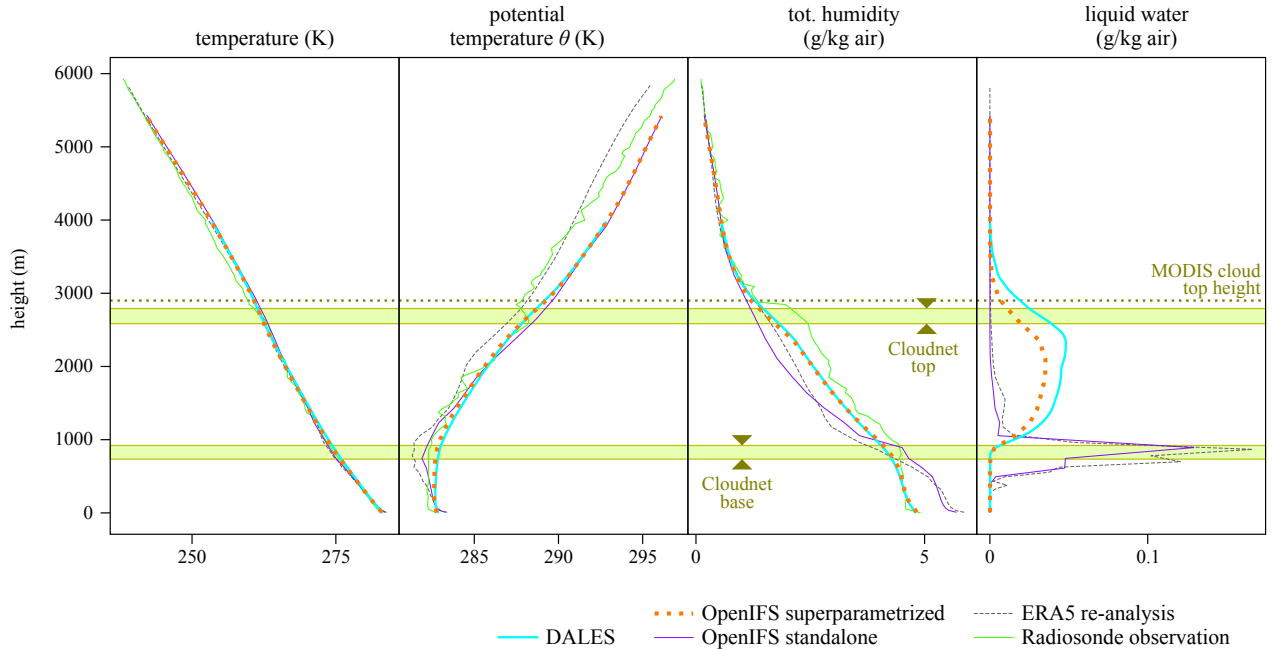
467 **Figure 6.** Zoom in on the superparameterized simulation and 3D views on selected local mod-
 468 els, compared to a satellite image from Terra / MODIS at 2012-04-13 11:35 UTC. The star marks
 469 de Bilt, where radiosonde observations were performed.

454 Figure 5 shows a snapshot of the superparameterized simulation, compared to a
 455 similar run of regular OpenIFS. Animations of the simulations shown are available as
 456 supplementary material. The state of the simulations are shown at 11:35 UTC, with the
 457 simulations initialized at midnight UTC the same day. This time was chosen to coincide
 458 with the overpass of the Terra satellite for comparison.

459 The figures illustrate the clouds in OpenIFS and in DALES through the liquid water
 460 path. Since the cloud optical thickness has a non-linear dependence on the liquid water
 461 path, we use a non-linear color map for the DALES instances, (a gamma correction
 462 with $\gamma = 1/2$, so the pixel coloring is determined by $(q_L/q_{L_{\max}})^\gamma$). The plot still of-
 463 fers only a crude approximation of how the clouds would actually appear on a satellite
 464 image, since the cloud optical thickness depends strongly on the droplet size distribu-
 465 tion, which is not taken into account in the plot. A more detailed quantitative compar-
 466 ison follows in section 4.2.

470 A magnification of the superparameterized run are shown in figure 6 together with
 471 a satellite image of the same area. As can be seen in the figure, the local models over
 472 land show more clouds than the ones over the sea, in agreement with the satellite im-
 473 age and reanalysis data. However, large, stratiform cloud fields are underrepresented in
 474 the superparametrized OpenIFS.

475 When comparing DALES cloud fields with observations, it is good to keep in mind
 476 that the local models in a superparameterized setup give a representation of the convec-
 477 tion and clouds at a grid point of the global model, but cannot be expected to accurately
 478 reproduce individual features or clouds seen in observations. One reason for this is that
 479 the initial state does not provide any small-scale information – the DALES simulations
 480 are initialized with vertical profiles from the global model. Secondly, the DALES sim-



484 **Figure 7.** Vertical profiles at 2012-04-13 12:00 UTC, of the grid point closest to de Bilt where
 485 radiosonde observations were performed. As a reference we use the ERA5 reanalysis and the
 486 KNMI radiosonde observations. The horizontal line shows the cloud top height retrieved from
 487 MODIS. The wide horizontal lines show the range of cloud top and cloud base heights a half-hour
 488 interval from Cloudnet, recorded by the cloud radar at the Cabauw site, 22 km Southwest of de
 489 Bilt.

481 simulations are performed with periodic boundary conditions, so that spatial coordinates
 482 in them do not directly correspond to any particular geographic coordinates.

483 4.2 Vertical profiles

490 Vertical profiles of temperature, humidity and liquid water humidity at a single OpenIFS
 491 grid point are shown in figure 7. The superparameterized run is shown with profiles from
 492 both DALES and the corresponding grid point in OpenIFS. It can be seen that in the
 493 superparameterized run, DALES and OpenIFS are consistent with each other as can be
 494 expected from the coupling scheme. The superparameterized run is compared to a similar
 495 run of the non-superparameterized OpenIFS, to the reanalysis from ERA5, and to
 496 radiosonde observations. The largest difference in results is seen in the liquid water
 497 profiles (right panel), where the superparameterization produces significantly higher clouds
 498 than standard OpenIFS. The superparameterization result agrees well with the cloud
 499 top height measurement of MODIS, 2900 m. Also the total humidity measured by the
 500 radiosonde shows a sharp step at this height, consistent with this being the cloud top
 501 height. We additionally compare the liquid water result with cloud radar recordings from
 502 Cloudnet (Illingworth et al., 2007), taken at the Cabauw site, 22 km Southwest of de Bilt.
 503 Over 30 minutes, the cloud top height was measured at 2690 ± 100 m, and the cloud
 504 base at 830 ± 90 m. These ranges are indicated with green stripes in figure 7, and show
 505 a good agreement with the liquid water results from the superparameterized simulation.

506 When comparing simulation results with re-analysis, one should remember that the
 507 reanalysis was done with IFS, of which OpenIFS is a version. There may thus be a bias

508 for the reanalysis to behave similar to OpenIFS. While the comparison presented here
 509 is certainly too limited to draw broad conclusions about the accuracy of the superpa-
 510 rameterized simulation, the match between the superparameterized clouds and MODIS,
 511 the radiosonde observations, and the Cloudnet cloud top and base heights is encourag-
 512 ing. At the same time the comparisons show that in particular the liquid water profiles
 513 from the reanalysis are inconsistent with the MODIS and Cloudnet observations. We note
 514 that the parameters of DALES have not been tuned for this comparison.

515 4.3 Performance

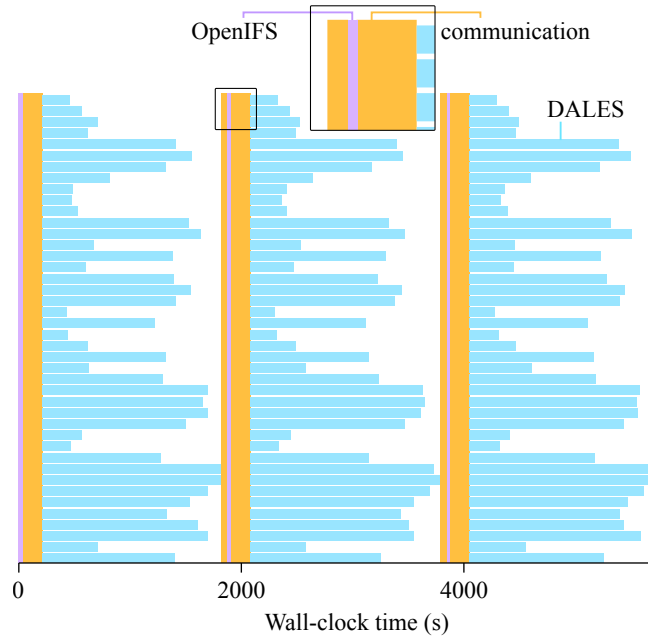
516 The superparameterized run with the 42 larger DALES models presented above,
 517 consisting of 21 hours of simulation and 4 hours of DALES spin-up, took 39 hours on
 518 ten nodes of the Cray-XC40 system at ECMWF. Each node in this system contains two
 519 18-core Intel Xeon EP E5-2695 V4 Broadwell processors. Each DALES instance used 8
 520 MPI tasks, resulting in 336 DALES processes in total. The first node ran the coupling
 521 script, OpenIFS with 17 processes, and 12 DALES processes. The remaining nine nodes
 522 ran 36 DALES processes each. The total cost of this simulation was 14041 core-hours.

523 Figure 8 shows the distribution of computing time over OpenIFS, the DALES mod-
 524 els and the communication, around the time of the snapshot shown in figure 5. Most of
 525 the time, 82 % is spent on the DALES models, followed by communication and coupling
 526 with 16 %. OpenIFS itself consumes only 2 % of the total time. There is considerable
 527 variation in the computational times for the different DALES instances, which appear
 528 since DALES uses adaptive time stepping. The more convection there is in a DALES
 529 volume, the shorter the time step needs to be, and the longer the simulation takes. This
 530 results in some work imbalance, since for each time step of the global model, the whole
 531 calculation must wait until the last DALES completes. If DALES would be parallelized
 532 with OpenMP in addition to the current MPI parallelization, it might be beneficial to
 533 dynamically adjust the number of tasks for each DALES instance to reduce the imbal-
 534 ance. Some further performance can most likely still be gained by carefully optimizing
 535 the job layout, and also by overlapping some of the communication steps with compu-
 536 tation. In the following section we address ways of accelerating the local models them-
 537 selves.

543 4.4 Acceleration

544 To reduce the computational cost of the superparameterized simulation, we con-
 545 sider ways of accelerating the local models, which consume most of the computational
 546 time. First, the horizontal extent of the local models may be chosen smaller than the
 547 global model’s grid size (Xing et al. (2009) calls this the ”reduced space strategy”). Global
 548 superparameterization studies have also frequently used this strategy, sometimes com-
 549 bined with making the local models 2-dimensional.

550 Second, the local models can be accelerated in time, using the mean state accel-
 551 eration method of Jones, Bretherton, and Pritchard (2015), which was also used in the
 552 superparameterization context by Parishani et al. (2017) with promising results. Briefly,
 553 this method assumes a separation of time scales, between the time of eddy motion (fast)
 554 and the time on which the local model’s horizontal averages change (slow). The tech-
 555 nique is a good match with superparameterization, since only the horizontal averages,
 556 with the slow time scale, are coupled to the global model. In the mean-state accelera-
 557 tion technique, after every time step in the local model, the horizontal averages of the
 558 tendencies are calculated. These average tendencies are then applied to the model vari-
 559 ables in a horizontally uniform way, in order to accelerate the rate of change for the hor-
 560 izontal means.

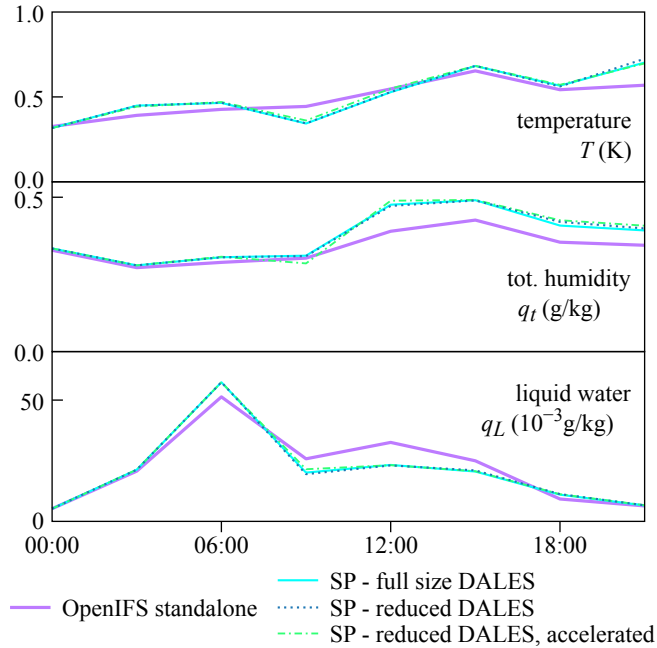


538 **Figure 8.** Timing diagram for the superparameterized run, showing three OpenIFS time steps
 539 around the time of the snapshot shown in figure 5. The blue horizontal bars show the wall-clock
 540 time required for each individual DALES instance to complete the time step. The vertical bars
 541 show the OpenIFS computation (purple) and communication between the coupler and the models
 542 (orange).

561 These techniques are demonstrated with two accelerated superparameterization runs
 562 with the same initial conditions as in the previous section. In the first, the horizontal
 563 extent of DALES is reduced to 64×64 columns, reducing the area to 10 % of the orig-
 564 inal. In the second run, the mean state acceleration is also applied, with an acceleration
 565 factor of 2. To evaluate the accuracy of the accelerated runs, we plot the RMS differ-
 566 ence between the global model variables and the ERA-5 reanalysis over time (figure 9).
 567 The plots show that the differences introduced by the acceleration are rather small.

571 The computational time requirements with and without acceleration are shown in
 572 table 3. Reducing the area covered by DALES to 10% of the original, reduces the DALES
 573 run time by a factor of 8.8. Adding mean-state acceleration with an acceleration
 574 factor of 2, further reduces the DALES runtime by a factor of 1.9. The total run time decreases
 575 less dramatically, by a factor 4 or 4.9, since the amounts of time spent on coupling and
 576 on OpenIFS remain constant. A simple way to decrease the time fraction spent on the
 577 coupling and communication is to allocate fewer processes per DALES - for this com-
 578 parison we kept the job layout the same for all runs. Another interesting optimization
 579 possibility is to increase the concurrency of computation in the model codes with com-
 580 munication between the coupler and the models.

584 These acceleration results seem promising for reducing the computational cost of
 585 superparameterization. We also note that the degrees of acceleration that can be achieved
 586 may depend on the case.



568 **Figure 9.** RMS difference between the superparameterized runs and the ERA-5 reanalysis,
 569 over all superparameterized grid points for the vertical levels up to the height of the DALES
 570 models.

LES grid	time acc.	run time (1000 s)				speedup factor	
		DALES	OpenIFS	coupler	total	DALES	total
$200 \times 200 \times 160$	-	115.4	2.6	22.0	140.0	1.0	1.0
$64 \times 64 \times 160$	-	13.1	2.6	19.2	34.9	8.8	4.0
$64 \times 64 \times 160$	2	6.9	2.6	19.2	28.7	16.7	4.9

581 **Table 3.** Comparison of the computational time for different parts of the simulation, with and
 582 without acceleration methods. All runs were performed as described in section 4.3, on the same
 583 computer system.

587 5 Conclusions and Outlook

588 We have demonstrated a superparameterization of a global atmospheric model with
 589 a three-dimensional, high-resolution atmospheric LES over a configurable region. We show
 590 an example with a 21 hour run where a region with an area of $240 \text{ km} \times 280 \text{ km}$ is su-
 591 perparameterized with high-resolution LES models. Reducing the extent of the local mod-
 592 els and applying mean-state acceleration drastically reduces the computational demands,
 593 with only minor deterioration of the results.

594 The coupling between the global and local models was implemented with a cou-
 595 pling program in Python, communicating with the model codes using the OMUSE frame-
 596 work. Implementing the coupler in Python as an independent program facilitated flex-
 597 ible development, while providing sufficient performance. Without acceleration meth-
 598 ods, the major part of the computation is spent on the local models. With the introduc-
 599 tion of acceleration methods for the local models, the performance increased to the point
 600 where the time spent in the coupler becomes significant, giving us a motivation to ad-
 601 dress the coupler performance in the future.

602 The simulation results demonstrate the potential of this approach. The cloudy re-
 603 gions, observed by MODIS are reproduced by the superparameterized grid boxes. Com-
 604 parison with the local observations at the Cabauw site shows that the superparameter-
 605 ized version of OpenIFS simulates a deeper convective mixing leading to improved pro-
 606 files of especially the specific humidity and the cloud amount, compared with the stan-
 607 dard version of the OpenIFS without superparameterization.

608 The simulations also illustrate limitations of this approach. As can be observed from
 609 Fig. 6, the superparameterized simulation poorly represents the observed coherent cloud
 610 structures of sizes comparable with or beyond the resolution of the global model (40 km).
 611 This is in part the consequence of the periodic boundary conditions of the local model
 612 and the lack of a direct coupling between the neighboring local model instances. This
 613 prevents the growth of mesoscale cloud structures, emerging from the smaller turbulent
 614 scales resolved in the local model, beyond the domain size of the local model. The cou-
 615 pling between the local and the global model, as expressed by Eq. (2) and Eq. (4), is ex-
 616 clusively formulated in terms of the mean values of the prognostic (thermo)dynamic vari-
 617 ables. Therefore, the coupling does not include any scale interaction of the variances of
 618 these variables, though many observational studies have shown a continuous growth of
 619 variances of temperature and humidity with the spatial scale as $\ell^{2/3}$, up to scales of sev-
 620 eral hundreds of kilometers without any scale break (Kahn et al., 2011). Work is there-
 621 fore in progress to introduce an additional coupling of the variances of the prognostic
 622 variables, guided by the behavior of the resolved variance and cloud amount of the global
 623 model (Cusack et al., 1999).

624 This present work and results demonstrate that employing LES models as super-
 625 parameterization is an attractive and efficient stepping stone toward global LES mod-
 626 eling which is relatively easy to implement in any existing global atmospheric model. More
 627 directly, it can also be used as an interactive zoom-in tool to obtain more accurate pre-
 628 dictions for high-impact areas such as large national airports or large wind energy and
 629 solar power farms. In addition there are numerous other useful applications of this frame-
 630 work more in the context of model development and analysis.

631 As already mentioned in the introduction, this framework can serve as a useful bench-
 632 mark for the development of new parameterized approaches. Many of the parameteri-
 633 zation developments of cloud related processes of the last twenty years have been guided
 634 by Large Eddy Simulations of relevant cases which are forced by realistic large-scale forc-
 635 ings (Brown et al., 2002; Siebesma et al., 2003; vanZanten et al., 2011). The present frame-
 636 work provides new opportunities in this respect. It provides realistic benchmarks over
 637 longer periods, over larger areas, with realistic forcings that are easy to set up. The frame-
 638 work also allows the use of different local models, e.g. an alternative parameterization
 639 package, data-driven algorithms trained by the LES (Dorrestijn et al., 2013; Schneider,
 640 Lan, et al., 2017), or conceptual mixed layer models (Caldwell et al., 2013). This way
 641 it is possible to test and compare different approaches which all are in balance with the
 642 large scales due to the interactive coupling.

643 By increasing the resolution of the global model and accordingly, reducing the do-
 644 main size of the local model, the present framework can also be used to quantify how
 645 the response of the local model will change. This will provide guidance for at which res-
 646 olutions and for which processes a scale-aware parameterizations are required. Such ex-
 647 periments will also be useful in exploring how mesoscale organization is emerging. By
 648 varying the resolution, the effect of imposing a scale break at different spatial scales on
 649 the mesoscale organization can be systematically explored.

Name	URL	Archived snapshot, DOI
sp-coupler	https://github.com/CloudResolvingClimateModeling/sp-coupler	10.5281/zenodo.1968305
OMUSE v1.1	https://bitbucket.org/omuse/omuse/	10.5281/zenodo.1407941
AMUSE	http://www.amusecode.org/	archived with OMUSE
Dales with OMUSE interface	https://github.com/CloudResolvingClimateModeling/dales	10.5281/zenodo.1345110
OpenIFS with OMUSE interface	https://git.ecmwf.int/scm/~g.vandenoord_esciencecenter.nl/oifs40r1-lib.git (requires license and a user account at ECMWF)	
OpenIFS, licensing information	https://confluence.ecmwf.int/display/OIFS	

650 **Table 4.** References for the different codes used in the superparameterization setup

651 Acknowledgments

652 We thank Glenn Carver at the ECMWF for help with OpenIFS and for providing us with
653 initial states for the simulation. We also thank Maria Chertova for comments on the manuscript
654 and Bram van Es for work on the setup and testing of the coupled model.

655 This work was supported by the Netherlands eScience Center (NLeSC) under grant
656 no. 027.015.G03. Furthermore, we acknowledge the use of ECMWF’s computing and archive
657 facilities in the research reported here. Also SURFsara provided computing resources.

658 The ERA5 and ERA-Interim data was provided by Copernicus Atmosphere Mon-
659 itoring Service information 2018. Neither the European Commission nor ECMWF is re-
660 sponsible for any use that may be made of the Copernicus Information or Data it con-
661 tains.

662 We acknowledge the use of imagery from the NASA Worldview application
663 (<https://worldview.earthdata.nasa.gov/>) operated by the NASA/Goddard Space
664 Flight Center Earth Science Data and Information System (ESDIS) project.

665 Radiosonde data was provided by KNMI. It was recorded with a Vaisala RS92 ra-
666 diosonde, released from de Bilt, the Netherlands.

667 The maps were drawn with Matplotlib (Hunter, 2007) and Basemap. The 3D cloud
668 images were raytraced in Blender.

669 Code Availability

670 All the codes required for the simulation are available under open-source licenses,
671 except OpenIFS (for which a license can be requested from ECMWF). Table 4 lists the
672 codes and URLs for repositories and DOI numbers for archived snapshots.

673 The top-level coupler code in Python is called sp-coupler. To run, it requires OMUSE
674 and versions of OpenIFS and DALES which include the OMUSE interfaces. For instal-
675 lation instructions, see the documentation in the coupler repository. The coupler repos-
676 itory includes a Singularity recipe. Singularity (Kurtzer et al., 2017) is a software con-
677 tainer system for scientific applications. The Singularity recipe is used to build a singu-
678 larity image — a self-contained unit containing all the programs and all their dependen-

679 cies needed to run the simulation. Building the Singularity image also requires access
680 to OpenIFS source code from ECMWF.

681 **Author contributions**

682 DC and PS conceived of the project. FJ, GvdO, DC, PS defined the coupling pro-
683 cedure. FJ, GvdO, IP wrote the coupling code and the OMUSE interfaces to DALES.
684 GvdO created the OMUSE interface to OpenIFS. FJ ran the simulations. JHG and FJ
685 developed the visualizations. JHG drew the figures. FJ wrote the article text, with con-
686 tributions and editing by all other authors.

687 **Appendix: Analysis of the coupling scheme**

688 Here we analyze the model coupling scheme in more detail. We show that the de-
689 sired equality (1) between the global and the (averaged) local model state is achieved
690 in cases where the advection and source terms are entirely situated either in the local
691 model or in the global model.

692 Consider steps (i) to (iv) of the superparameterization scheme given in section 2.
693 Combining (i) and (ii) gives

$$Q(T + \Delta T) = \langle q(T) \rangle + \Delta T (A_Q(T) + S_Q(T)). \quad (14)$$

694 In (iv), $f_q(T)$ does not change with t , and thus $\sum_{t=T}^{T+\Delta T} \Delta t f_q(T) = \Delta T f_q$. With (iii)
695 and (iv), this leads to $q(T + \Delta T) = q(T) + Q(T + \Delta T) - \langle q(T) \rangle + \sum_{t=T}^{T+\Delta T} \Delta t (a_q(t) +$
696 $s_q(t))$. Taking the horizontal average we find

$$\langle q(T + \Delta T) \rangle = Q(T + \Delta T) + \sum_{t=T}^{T+\Delta T} \Delta t \langle a_q(t) + s_q(t) \rangle. \quad (15)$$

697 In general, $Q(T) \neq \langle q(T) \rangle$ and $Q(T + \Delta T) \neq \langle q(T) \rangle$, as can be seen from the identi-
698 ties just derived. Thus, the equality (1) is generally not satisfied. However, if all of the
699 advection and sources with nonzero average are accounted for in one model (global or
700 local) and none in the other, the equality is satisfied (albeit possibly in a time-lagged sense).
701 More precisely, assume $A_Q(T) + S_Q(T) = 0$, i.e. all advection and sources are in the
702 local model. Then $Q(T + \Delta T) = \langle q(T) \rangle$ by construction. Conversely, if the local model
703 has no advection or source terms with nonzero horizontal average, so that $\langle a_q(t) + s_q(t) \rangle =$
704 0 for all t , we have $\langle q(T + \Delta T) \rangle = Q(T + \Delta T)$.

705 If both $A_Q(T) + S_Q(T) \neq 0$ and $\langle a_q(t) + s_q(t) \rangle \neq 0$, we can consider the differ-
706 ence between $Q(T + \Delta T)$ on the one hand and a weighted average of $\langle q(T) \rangle$ and $\langle q(T +$
707 $\Delta T) \rangle$ on the other hand. Defining the weighting parameter α with $0 \leq \alpha \leq 1$, we have

$$Q(T) - (\alpha \langle q(T) \rangle + (1 - \alpha) \langle q(T + \Delta T) \rangle) = \alpha \Delta T (A_Q(T) + S_Q(T)) - (1 - \alpha) \sum_{t=T}^{T+\Delta T} \Delta t \langle a_q(t) + s_q(t) \rangle. \quad (16)$$

708 The RHS equals zero if $\Delta T (A_Q(T) + S_Q(T))$ and $\sum_{t=T}^{T+\Delta T} \Delta t \langle a_q(t) + s_q(t) \rangle$ have the
709 same sign and their ratio equals $(1 - \alpha)/\alpha$. To satisfy the latter requirement, α must
710 depend on time T , vertical level z and prognostic variable q, Q .

711 **References**

712 Bony, S., Stevens, B., Frierson, D. M. W., Jakob, C., Kageyama, M., Pincus, R., . . .
713 Webb, M. J. (2015, mar). Clouds, circulation and climate sensitivity. *Nature*
714 *Geoscience*, 8, 261. doi: 10.1038/ngeo2398

- 715 Bretherton, C. S., & Khairoutdinov, M. F. (2015). Convective self-aggregation
716 feedbacks in near-global cloud-resolving simulations of an aquaplanet.
717 *Journal of Advances in Modeling Earth Systems*, 7(4), 1765-1787. doi:
718 10.1002/2015MS000499
- 719 Brown, A. R., Cederwall, R. T., Chlond, A., Duynkerke, P. G., Golaz, J.-C.,
720 Khairoutdinov, M., ... Stevens, B. (2002). Large-eddy simulation of
721 the diurnal cycle of shallow cumulus convection over land. *Quarterly*
722 *Journal of the Royal Meteorological Society*, 128(582), 1075-1093. doi:
723 10.1256/003590002320373210
- 724 Caldwell, P. M., Zhang, Y., & Klein, S. A. (2013). Cmp3 subtropical stratocumulus
725 cloud feedback interpreted through a mixed-layer model. *Journal of Climate*,
726 26(5), 1607-1625. doi: 10.1175/JCLI-D-12-00188.1
- 727 Carver, G., & Vana, F. (2017). Openifs home. """ Retrieved from [https://
728 software.ecmwf.int/wiki/display/OIFS/OpenIFS1Home](https://software.ecmwf.int/wiki/display/OIFS/OpenIFS1Home)
- 729 Cusack, S., Edwards, J. M., & Kershaw, R. (1999). Estimating the subgrid variance
730 of saturation, and its parametrization for use in a gcm cloud scheme. *Quar-*
731 *terly Journal of the Royal Meteorological Society*, 125(560), 3057-3076. doi:
732 10.1002/qj.49712556013
- 733 Dee, D. P., Uppala, S. M., Simmons, A. J., Berrisford, P., Poli, P., Kobayashi, S., ...
734 Vitart, F. (2011). The ERAInterim reanalysis: configuration and performance
735 of the data assimilation system. *Quarterly Journal of the Royal Meteorological*
736 *Society*, 137(656), 553-597. doi: 10.1002/qj.828
- 737 Dorrestijn, J., Crommelin, D. T., Siebesma, A. P., & Jonker, H. J. (2013). Stochas-
738 tic parameterization of shallow cumulus convection estimated from high-
739 resolution model data. *Theoretical and Computational Fluid Dynamics*,
740 27(1-2), 133-148. doi: 10.1007/s00162-012-0281-y
- 741 Grabowski, W. W. (2001). Coupling cloud processes with the large-scale dynamics
742 using the cloud-resolving convection parameterization (CRCP). *Journal of the*
743 *Atmospheric Sciences*, 58(9), 978-997. doi: 10.1175/1520-0469(2001)058<0978:
744 CCPWTL>2.0.CO;2
- 745 Grabowski, W. W. (2004). An improved framework for superparameteri-
746 zation. *Journal of the Atmospheric Sciences*, 61(15), 1940-1952. doi:
747 10.1175/1520-0469(2004)061<1940:AIFFS>2.0.CO;2
- 748 Grabowski, W. W. (2016). Towards global large eddy simulation: Super-
749 parameterization revisited. *Journal of the Meteorological Society of Japan.*
750 *Ser. II*, 94(4), 327-344. doi: 10.2151/jmsj.2016-017
- 751 Grabowski, W. W., & Smolarkiewicz, P. K. (1999). CRCP: a cloud resolv-
752 ing convection parameterization for modeling the tropical convecting at-
753 mosphere. *Physica D: Nonlinear Phenomena*, 133(1- 4), 171 - 178. doi:
754 10.1016/S0167-2789(99)00104-9
- 755 Heinze, R., Dipankar, A., Henken, C. C., Moseley, C., Sourdeval, O., Trmel, S., ...
756 Quaas, J. (2017). Large-eddy simulations over germany using icon: a com-
757 prehensive evaluation. *Quarterly Journal of the Royal Meteorological Society*,
758 143(702), 69-100. doi: 10.1002/qj.2947
- 759 Heus, T., van Heerwaarden, C. C., Jonker, H. J. J., Pier Siebesma, A., Axelsen,
760 S., van den Dries, K., ... Vilà-Guerau de Arellano, J. (2010). Formulation
761 of the Dutch Atmospheric Large-Eddy Simulation (DALES) and overview
762 of its applications. *Geoscientific Model Development*, 3(2), 415-444. doi:
763 10.5194/gmd-3-415-2010
- 764 Hunter, J. D. (2007). Matplotlib: A 2d graphics environment. *Computing In Science*
765 *& Engineering*, 9(3), 90-95. doi: 10.1109/MCSE.2007.55
- 766 Illingworth, A. J., Hogan, R. J., O'Connor, E., Bouniol, D., Brooks, M. E., De-
767 lano, J., ... Wrench, C. L. (2007). Cloudnet: Continuous evaluation
768 of cloud profiles in seven operational models using ground-based observa-
769 tions. *Bulletin of the American Meteorological Society*, 88(6), 883-898. doi:

- 770 10.1175/BAMS-88-6-883
- 771 Jones, C. R., Bretherton, C. S., & Pritchard, M. S. (2015). Mean-state acceleration
772 of cloud-resolving models and large eddy simulations. *Journal of Advances in*
773 *Modeling Earth Systems*, 7(4), 1643-1660. doi: 10.1002/2015MS000488
- 774 Jung, J., & Arakawa, A. (2010). Development of a quasi3d multiscale modeling
775 framework: Motivation, basic algorithm and preliminary results. *Journal of*
776 *Advances in Modeling Earth Systems*, 2(4). doi: 10.3894/JAMES.2010.2.11
- 777 Kahn, B. H., Teixeira, J., Fetzer, E. J., Gettelman, A., Hristova-Veleva, S. M.,
778 Huang, X., ... Zhao, M. (2011). Temperature and water vapor variance scal-
779 ing in global models: Comparisons to satellite and aircraft data. *Journal of the*
780 *Atmospheric Sciences*, 68(9), 2156-2168. doi: 10.1175/2011JAS3737.1
- 781 Khairoutdinov, M., Randall, D., & DeMott, C. (2005). Simulations of the atmo-
782 spheric general circulation using a cloud-resolving model as a superparame-
783 terization of physical processes. *Journal of the Atmospheric Sciences*, 62(7),
784 2136-2154. doi: 10.1175/JAS3453.1
- 785 Khairoutdinov, M., & Randall, D. A. (2001). A cloud resolving model as a
786 cloud parameterization in the NCAR community climate system model:
787 Preliminary results. *Geophysical Research Letters*, 28(18), 3617-3620. doi:
788 10.1029/2001GL013552
- 789 Kurtzer, G. M., Sochat, V., & Bauer, M. W. (2017, 05). Singularity: Scientific con-
790 tainers for mobility of compute. *PLOS ONE*, 12(5), 1-20. doi: 10.1371/journal
791 .pone.0177459
- 792 Marchand, R., & Ackerman, T. (2011). A cloud-resolving model with an adaptive
793 vertical grid for boundary layer clouds. *Journal of the Atmospheric Sciences*,
794 68(5), 1058-1074. doi: 10.1175/2010JAS3638.1
- 795 Miyamoto, Y., Kajikawa, Y., Yoshida, R., Yamaura, T., Yashiro, H., & Tomita, H.
796 (2013). Deep moist atmospheric convection in a subkilometer global simula-
797 tion. *Geophysical Research Letters*, 40(18), 4922-4926. doi: 10.1002/grl.50944
- 798 Neggers, R. A. J., Heus, T., & Siebesma, A. P. (2011). Overlap statistics of cu-
799 muliform boundary-layer cloud fields in large-eddy simulations. *Journal of*
800 *Geophysical Research: Atmospheres*, 116(D21). doi: 10.1029/2011JD015650
- 801 Parishani, H., Pritchard, M. S., Bretherton, C. S., Wyant, M. C., & Khairoutdinov,
802 M. (2017). Toward low-cloud-permitting cloud superparameterization with
803 explicit boundary layer turbulence. *Journal of Advances in Modeling Earth*
804 *Systems*, 9(3), 1542-1571. doi: 10.1002/2017MS000968
- 805 Pelupessy, I., van Werkhoven, B., van Elteren, A., Viebahn, J., Candy, A., Portegies
806 Zwart, S., & Dijkstra, H. (2017). The oceanographic multipurpose software en-
807 vironment (omuse v1.0). *Geoscientific Model Development*, 10(8), 3167-3187.
808 doi: 10.5194/gmd-10-3167-2017
- 809 Pelupessy, F. I., van Elteren, A., de Vries, N., McMillan, S. L. W., Drost, N., &
810 Portegies Zwart, S. F. (2013). The astrophysical multipurpose software envi-
811 ronment. *A&A*, 557, A84. doi: 10.1051/0004-6361/201321252
- 812 Portegies Zwart, S., McMillan, S., Harfst, S., Groen, D., Fujii, M., Ó Nualláin, B.,
813 ... Zemp, M. (2009). A multiphysics and multiscale software environment
814 for modeling astrophysical systems. *New Astronomy*, 14(4), 369 - 378. doi:
815 https://doi.org/10.1016/j.newast.2008.10.006
- 816 Portegies Zwart, S. F., McMillan, S. L., van Elteren, A., Pelupessy, F. I., & de Vries,
817 N. (2013). Multi-physics simulations using a hierarchical interchangeable
818 software interface. *Computer Physics Communications*, 184(3), 456 - 468. doi:
819 https://doi.org/10.1016/j.cpc.2012.09.024
- 820 Schalkwijk, J., Jonker, H. J. J., Siebesma, A. P., & Van Meijgaard, E. (2015).
821 Weather forecasting using gpu-based large-eddy simulations. *Bulletin*
822 *of the American Meteorological Society*, 96(5), 715-723. doi: 10.1175/
823 BAMS-D-14-00114.1
- 824 Schneider, T., Lan, S., Stuart, A., & Teixeira, J. (2017). Earth system modeling

- 825 2.0: A blueprint for models that learn from observations and targeted high-
 826 resolution simulations. *Geophysical Research Letters*, 44(24), 12,396-12,417.
 827 doi: 10.1002/2017GL076101
- 828 Schneider, T., Teixeira, J., Bretherton, C. S., Brient, F., Pressel, K. G., Schär, C., &
 829 Siebesma, A. P. (2017, January). Climate goals and computing the future of
 830 clouds. *Nature Climate Change*, 7, 3-. doi: 10.1038/nclimate3190
- 831 Siebesma, A. P., Bretherton, C. S., Brown, A., Chlond, A., Cuxart, J., Duynkerke,
 832 P. G., ... Stevens, D. E. (2003). A large eddy simulation intercomparison
 833 study of shallow cumulus convection. *Journal of the Atmospheric Sciences*,
 834 60(10), 1201-1219. doi: 10.1175/1520-0469(2003)60<1201:ALESIS>2.0.CO;2
- 835 Tao, W., & Chern, J. (2017). The impact of simulated mesoscale convective systems
 836 on global precipitation: A multiscale modeling study. *Journal of Advances in*
 837 *Modeling Earth Systems*, 9(2), 790-809. doi: 10.1002/2016MS000836
- 838 vanZanten, M. C., Stevens, B., Nuijens, L., Siebesma, A. P., Ackerman, A. S., Bur-
 839 net, F., ... Wyszogrodzki, A. (2011). Controls on precipitation and cloudiness
 840 in simulations of trade-wind cumulus as observed during rico. *Journal of*
 841 *Advances in Modeling Earth Systems*, 3(2). doi: 10.1029/2011MS000056
- 842 Xing, Y., Majda, A. J., & Grabowski, W. W. (2009). New efficient sparse space-time
 843 algorithms for superparameterization on mesoscales. *Monthly Weather Review*,
 844 137(12), 4307-4324. doi: 10.1175/2009MWR2858.1